Fractionating Condensation and Evaporation in Plate-Fin Devices

A model that describes fractionation with condensation and evaporation in a plate-fin device has been formulated. It is capable of evaluating profiles of composition, temperature, and flow rate for both liquid and vapor streams in an extended surface device. The device may be adiabatic or nonadiabatic and the surface may be incompletely wetted. Compared to experimental measurements, the model predictions showed ±1 number of transfer unit deviation along the length of the device. The predictions of the top and bottom flow rate ratio showed a 5-10% deviation for adiabatic and condensation runs and a 25% deviation for evaporation runs.

Hsien-Hsin Tung, J. F. Davis, R. S. H. Mah
Department of Chemical Engineering
Northwestern University
Evanston, IL 60201

SCOPE

Fractionation processes are generally operated under adiabatic conditions and with very low thermodynamic efficiencies. Rising energy costs since the early 1970's have created substantial incentives for improving the efficiencies of these processes (Henley and Seader, 1981; Schluter and Schmidt, 1983). Nonadiabatic operation is one modification proposed to improve the efficiency of distillation. A distillation scheme that makes use of secondary reflux and vaporization (SRV) to enhance its thermal efficiency has shown considerable promise based on simulation results (Mah et al. 1977; Fitzmorris and Mah, 1980). Among several possible methods for implementing the SRV concept, a plate-fin device has shown to be one promising realization (Mah, 1981). In a plate-fin device, alternate and adjacent vertical channels serve as strippers and rectifiers. Because of the large amount of fin surface area available for both heat and mass transfer, SRV distillation could be operated in an integrated piece of equipment with a low-temperature driving force between the rectifying sections and stripping sections. Since heat is transfered from the rectifying sections to the stripping sections, fractionation is accompanied by substantial condensation or evaporation along the length of the column. To describe properly the performance of a plate-fin device, it is crucial that the design model should consider the heat and mass transfer simultaneously under nonadiabatic conditions.

In the study of nonadiabatic fractionation in continuous contact devices, previous studies were mostly confined to the wetted-wall column. A thorough literature search and detailed study of nonadiabatic fractionation in a wetted-wall column has been presented in our previous paper (Davis et al., 1984); therefore additional referencing is not made here. In the previous paper, a model was developed to describe falling film fractionators with evaporation and condensation. Film theory was used in the vapor phase to account for the effect of large mass flux across the vapor-liquid interface. Zero mass transfer resistance and linear temperature profile were assumed in the liquid film. In spite of its simplicity, the predictions showed strong agreement with experimental data. As to other types of devices, Watanabe and Munakata (1976) have simulated the behavior of a packed column with external heating or cooling. However the analysis was based upon either constant mass transfer coefficient or constant height of transfer unit (HTU). Another type of device, called an overflow packed column, has been studied by Haselden et al. (1960), Platt and Haselden

Correspondence concerning this paper should be addressed to R. S. H. Mah.
Hsien-Hsin Tung is now with the Chemical Engineering Department, California Institute of Technology.
James F. Davis is now with the Department of Chemical Engineering, The Ohio State University.

(1965), and Winteringham and Haselden (1966). Their results showed a 70% deviation of HTU for condensation runs and 100% deviation of HTU for evaporation runs between the predictions and the experimental data (Winteringham and Haselden).

In this paper, we shift our attention from the wetted-wall column to the plate-fin device. Our objectives are first to identify model features that represent significant departures from the wetted-wall model, and second to develop a computing procedure for a plate-fin device. Evaporation and condensation experiments, as well as adiabatic experiments, were performed in two rectangular offset plate-fin devices. Comparison between the predictions and the experimental data was made in terms of number of transfer units (NTU's) and flow rate ratio.

CONCLUSIONS AND SIGNIFICANCE

A model has been developed to describe fractionation with condensation and evaporation in a plate-fin device. It extends the wetted-wall model (Davis et al., 1984) by incorporating three important factors: wetted ratio, ω, which is defined as the wet fin surface area over total fin surface area, wall heat flux distribution between the dry and wet fin surface, and fin efficiency. The model allows us to calculate profiles of composition, temperature, and flow rate of the liquid and vapor streams in an extended-surface device. The device may be operated under adiabatic or nonadiabatic conditions and the surface may be incompletely wetted. Because incomplete wetting affects strongly the performance of the device, the proposed model presents a more realistic and satisfactory approach for the plate-fin device than the wetted-wall model.

Two plate-fin devices were constructed for both condensation and evaporation experiments. *N*-hexane and toluene were used. The experiments were run under total reflux conditions with a maximum composition difference of 90% mole fraction, corresponding to about 6 NTU's, and a maximum flow rate variation of sixfold across the length of the column. Vapor composition profiles and top and bottom flow rates were measured.

By assuming that the wetted ratio can be calculated by Eq. 19, that dry wall heat flux is negligible, and that fin efficiency is equal to 1, the predictions showed a ± 1 NTU deviation along the length of the column, 5-10% deviation in flow rate ratio for the adiabatic and condensation runs, and 25% deviation for the evaporation runs. Since significant entrance effects prevented reliable direct measurement of the boundary conditions, theoretical predictions required estimated values to compute NTU profiles. Because of this, the ± 1 NTU deviation is not considered substantial. The deviation in the flow rate ratio of the evaporation runs is believed to be caused by neglecting the dry wall heat flux. Since an electrical heater was used to supply wall heat during evaporation runs, this approximation would overpredict the flow rate ratio. For adiabatic or condensation runs, much better agreement was obtained.

Based upon the comparison with experimental results, it is concluded that the model has identified the major features in modeling the plate-fin device. Due to the generality of the proposed model, it is expected to be applicable to other types of extended surface devices.

Description of Plate-Fin Devices

Figure 1 illustrates the configuration of a rectangular offset plate-fin device. During operation, liquid enters the top of the column and flows downward along the fin surface. Vapor enters the bottom of the column and flows upward through the fin passages. Heat is added or removed through the primary wall. Fractionation with condensation and evaporation occurs continuously along the length of the column. To model this process, we can view each small uninterrupted fin passage as a small wetted-wall column. In this way, we can develop an extended model based upon the wetted-wall analysis. However, the plate-fin device has certain characteristics that do not exist in the wetted-wall column. Thus, a deeper examination of the system is necessary.

The first distinctive feature of the plate-fin device is the incomplete wetting of the fin surface, a phenomenon that commonly occurs in packed column operation (Puranik and Vogelpohl, 1974). Incomplete wetting occurs because the small hydraulic diameter of the fin passages lowers the flooding limit significantly. Thus the allowable liquid flow rate becomes insufficient to wet the entire fin surface. Consequently, less vapor-liquid interfacial area is available for mass diffusion. Furthermore, if there is a significant amount of condensation or evaporation, the wetted area can vary substantially along the length of the column.

Heat transfer is also affected strongly by this phenomenon. Wall heat flux across dry and wet fin surfaces is uneven because of the difference in heat transfer ability of the liquid and vapor streams. In addition, the extended heat transfer surface requires the consideration of fin efficiency to account for the temperature gradients in the wet fin region (Burmester, 1982; Nader, 1978; Patankar and Sparrow, 1979), and possibly in the dry fin region as well.

There are other complications. In the vapor phase, boundary layers of momentum, temperature, and composition are repeatedly generated at the leading edges of fin strips, giving rise to enhanced rates of heat and mass transfer (Sparrow et al., 1977). In addition, liquid leaving the trailing edges of fin strips can fall into the vapor phase directly, causing entrainment. The subse-

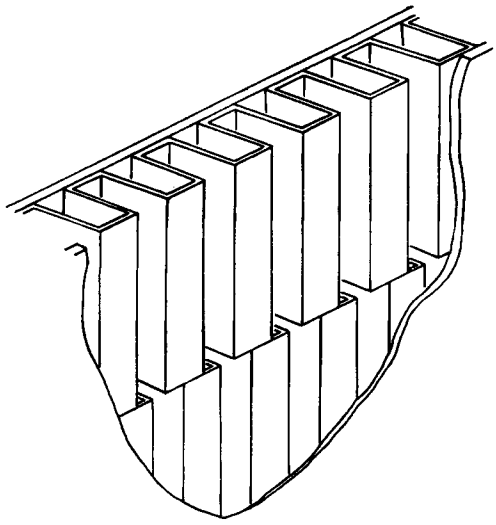

Figure 1. Rectangular offset plate-fin device.

quent fin surface becomes dry because no liquid is available, hence less fin surface is wetted. However, the effect of this complication is speculated to be minor, because the entrained liquid still provides additional vapor-liquid interfacial area for mass diffusion. It is also possible that the entrained liquid would redeposit in a relatively short distance due to the eddy turbulence in the vapor phase. For this reason, entrainment effect is not considered in the following derivation.

Mathematical Model

The fin surface can be divided into two regions: a wet region and a dry region, Figure 2. In the wet region, heat and mass transfer take place across the vapor-liquid interface, but heat transfer only takes place across the solid-liquid interface. In the dry region, heat transfer only takes place across the solid-vapor interface. Let us define ω as the ratio of wet fin surface area to the total fin surface area. The total material balance, component material balance, and energy balance along the z direction can be written as follows:

$$\frac{dV}{dz} = (n_1 + n_2)Aa_f\omega \tag{1}$$

$$\frac{dL}{dz} = -\frac{dV}{dz} \tag{2}$$

$$\frac{d(Vy)}{dz} = n_1 Aa_f\omega \tag{3}$$

$$\frac{d(Lx)}{dz} = -\frac{d(Vy)}{dz} \tag{4}$$

$$\frac{d(VH)}{dz} = Aa_f(\omega e + (1 - \omega)q_{w,dry}) \tag{5}$$

$$\frac{d(Lh)}{dz} = -\frac{d(VH)}{dz} + q_w Aa_f \tag{6}$$

where $q_{w,dry}$ is the dry wall heat flux, and q_w is the average wall heat flux.

In order to solve Eqs. 1–6, additional equations are needed to evaluate n_1, n_2, ω, e, and $q_{w,dry}$ with given boundary conditions of V, L, x, y, T, and t at either end of the column, and q_w along the length of the column.

Heat and mass transfer in the liquid phase

For laminar flow with the assumptions of negligible interfacial shear, linear temperature profile, and zero mass transfer resistance in the liquid film (Davis et al., 1984), we obtain:

$$x_i = x \tag{7}$$

$$q_{w,wet} = h_l\eta(t_{w,wet} - t_i) \tag{8}$$

$$h_l = \left(\frac{\kappa_l^3 g\rho_l^3 Aa_f}{3LM_l\mu_l}\right)^{1/3} \tag{9}$$

where η is the fin efficiency.

Heat and mass transfer in the vapor phase

Because of flooding limitations, the vapor flow rate will lie in the laminar and transition regions (based on a hydraulic diameter). Correlations for the heat transfer coefficients are given by Chapman (1974):

$$h_g = 1.86WMc_p(d/l)^{1/3}\,Pr^{-2/3}\,Re^{-2/3}; \quad Re \le 1{,}000$$
$$h_g = 0.036WMc_p(d/l)^{1/18}\,Pr^{-2/3}\,Re^{-.2}; \quad Re \ge 2{,}000 \tag{10}$$

A linear relationship is assumed in the transition region.

Other correlations are also available (Weiting, 1975). However, Eq. 10 and Weiting's correlation yield similar results under the current experimental conditions (Tung, 1985). Equation 10, which is valid for flows in finite tube length, was used in the computation because it is more general than Weiting's correlation, which is valid only for flows in a set of rectangular offset plate-fin devices.

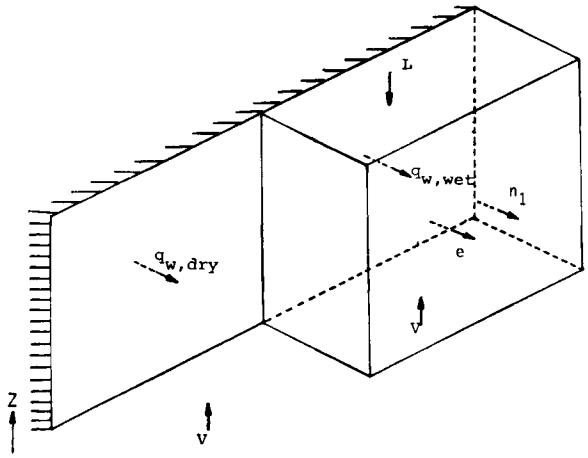

Figure 2. Heat and mass transfer in the wet and dry regions.

Mass transfer coefficients are obtained through the Chilton-Colburn analogy:

$$k_g = \left(\frac{h_g}{Mc_p W}\right)\left(\frac{Pr}{Sc}\right)^{2/3} \tag{11}$$

These coefficients are corrected for a finite mass flux across the vapor-liquid interface using film theory. The corrected expressions are:

$$k_g^* = k_g\Phi/(e^{\Phi} - 1); \quad \Phi = (n_1 + n_2)k_g \tag{12}$$

$$h_g^* = h_g\Psi/(e^{\Psi} - 1); \quad \Psi = (n_1 c_{p,1} M_1 + n_2 c_{p,2} M_2)/h_g \tag{13}$$

Conditions at the vapor-liquid interface

The following equations are imposed by phase equilibrium at the interface:

$$t_i = t_i(x_i, p) \tag{14}$$

$$y_i = y_i(T_i, p) \tag{15}$$

$$T_i = t_i \tag{16}$$

Taking into account a nonzero net mass flux across the vapor-liquid interface, the component material balance and energy balance yield:

$$n_1 = k_g^*(y_i - y) + y_i(n_1 + n_2) \tag{17}$$

and

$$q_{w,wet} + n_1 h_1 + n_2 h_2 = h_g^*(T_i - T) + n_1 H_1 + n_2 H_2 = e$$
$$q_{w,wet} = h_g^*(T_i - T) + n_1\lambda_1 + n_2\lambda_2 \tag{18}$$

Wetted ratio, wall heat distribution, and fin efficiency

The wetted ratio is estimated by:

$$\omega = L/(Aa_f\Gamma); \quad q_w \geq 0$$
$$\omega = 1.5L/(Aa_f\Gamma); \quad q_w < 0 \tag{19}$$

where ω is less than or equal to 1, and Γ is the minimum wetting rate. Ponter's correlation (Ponter et al., 1967) was used to compute the Γ:

$$\Gamma = 1.12(1 - \cos\theta)^{0.6}\left(\frac{\rho_l\gamma_l^3\mu_l}{g}\right)^{0.2} M_l^{-1} \tag{20}$$

Equation 19 is arrived at based upon the definition of minimum wetting rate. Minimum wetting rate is defined as the minimum liquid flow rate needed to keep the liquid in a continuous film. Therefore, knowing the liquid flow rate, we can easily calculate the maximum wetted surface by dividing the liquid flow rate with minimum wetting rate. A better fit of the experimental data was obtained by introducing a factor of 1.5 in the condensation condition. Dropwise condensation on the "dry" fin surface may provide a qualitative explanation. Since, during the condensation, the dry wall temperature will be lower than the dew point temperature, it is possible that liquid drops will form, coalesce and flow down the "dry" surface periodically (Rao and Murthy, 1983). Hence the actual wet fin surface area would be higher than that calculated from minimum wetting rate.

In calculating the wetted ratio, the effects of contact angle and surface tension at the boundaries of dry and wet regions have been neglected. As a matter of fact, theoretical analyses (Bankoff and Tung, 1982; Mikielewicz and Moszynski, 1976) have usually assumed that the film will break into equally spaced rivulets each with a cross section in the shape of a segment of a circle. However, these analyses have only reached limited success. Experimental observation tends to suggest that these rivulets coalesce after they are formed (Fujuta and Ueda, 1978). Therefore it seems reasonable to ignore the effects of contact angle and surface tension.

The wall heat flux distribution and fin efficiency are two closely related quantities. An energy balance across the fin surface is readily written as:

$$q_w = \omega q_{w,wet} + (1 - \omega)q_{w,dry} \tag{21}$$

However, the distribution of $q_{w,wet}$ and $q_{w,dry}$ depends strongly on the geometry of the device, local liquid and vapor flow patterns, and the boundary conditions at the primary wall. It would be very difficult, if not impossible, to estimate these quantities accurately. Since liquid has a much higher heat transfer ability than that of vapor, we assume that $q_{w,dry}$ is negligible in comparison with $q_{w,wet}$:

$$q_{w,dry} = 0 \tag{22}$$

The consequence of this assumption will be discussed in more detail in the section on comparison of results.

Exact calculation of the fin efficiency has a similar difficulty. Nevertheless, we have calculated its value under the experimental conditions using the equations of Kern and Kraus (1972, pp. 391–396). Assuming that there is only a vapor phase, the efficiency was found generally close to 1 (Tung, 1985). Since liquid has a much higher heat transfer ability than vapor, it is considered proper to assume that the fin efficiency is equal to 1 in our analysis:

$$\eta = 1 \tag{23}$$

Computing Procedure

The model developed in the previous section was used to compute the behavior of a plate-fin device under adiabatic and nonadiabatic conditions. The integration can start from either end of the column. Boundary conditions required are vapor and liquid temperatures, compositions, and flow rates. In addition, the average wall heat flux, column length, fin passage hydraulic diameter, fin strip length, and operating pressure must be specified.

The computation proceeds according to the following procedure:

1. Calculate physical properties of vapor and liquid streams. The properties include vapor pressure, latent heat, heat capacity, viscosity, diffusivity, thermal conductivity, and density. The methods used are given in Davis et al. (1984).
2. Evaluate k_g and h_g using Eqs. 10 and 11.
3. Evaluate x_i, y_i, t_i, and T_i by Eqs. 7, and 14–16.
4. Calculate ω, $q_{w,wet}$ and $t_{w,wet}$ by Eqs. 8, 9, and 19–23.

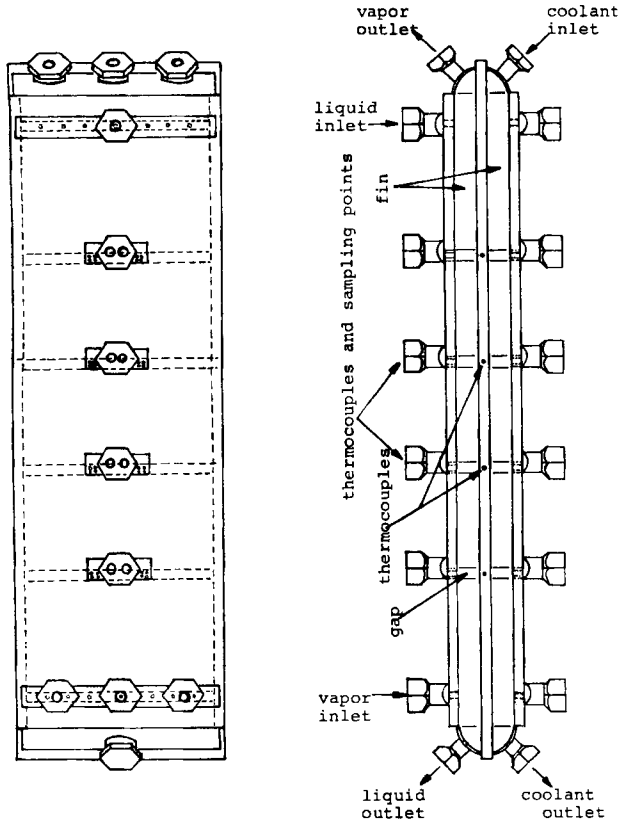

Figure 3. Double-channel plate-fin device.

5. Calculate n_1 and n_2 by solving Eqs. 17 and 18 iteratively, along with Eqs. 12 and 13. An iteration is started by first guessing a value for the sum $n_1 + n_2$. Individual values of n_1 and n_2 are then calculated with Eq. 17. The correct values are obtained when Eq. 18 is satisfied.

6. Integrate Eqs. 1–6 to obtain profiles of V, L, y, x, T, and t.

Adams' method found in the IMSL subroutine DGEAR was used for the integration.

Experimental Unit and Operation

Two plate-fin devices, a single-channel and a double-channel device with identical channel configurations, were constructed by Trane Company, La Crosse, Wisconsin. Figure 3 shows the double-channel plate-fin device and Table 1 summarizes the geometrical quantities. The single-channel device was built for evaporation experiments as well as adiabatic experiments. Heat was supplied externally through the wall by a strip heater with 900 W capacity. The double-channel device was built for condensation experiments. Heat was removed by cooling water that flowed downward in the adjacent channel.

Table 1. Geometrical Quantities of Plate-Fin Devices

Column length	0.953 m
Column width	0.203 m
Column gap	0.00965 m
Column cross area	0.00196 m^2
Fin height	0.00965 m
Fin width	0.0031 m
Fin strip	0.0508 m
Hydraulic dia.	0.0047 m

Along the column length there are four sampling points. At each sampling point the fin section has a gap to ensure complete mixing of the vapor and liquid from all fin passages. A small chamber that acts as a vapor-liquid separator is provided for knocking out any liquid that is entrained in the vapor sample. Compositions were taken along the column length in order to calculate the NTU profile. In parallel with the sampling points there are four wall-temperature measurement positions, as shown in Figure 3. Two of these measurement positions, the first and the third from the column top, contain two thermocouples for observing the variation in wall temperature due to incomplete wetting of the fin surface. Vapor and liquid enter the column through the headers. Even distribution across the width relies solely on the headers and the offset fin design. Entrance effects are unavoidable.

Under a pressure of 1.0135×10^5 Pa with equal composition of *n*-hexane and toluene, the flooding limit was estimated to be 1.15×10^{-4} kmol/s under total reflux conditions (Hewitt and Hall-Taylor, 1970, p. 72). Under the same conditions, the minimum liquid flow rate was estimated to be 1.3×10^{-4} kmol/s (Ponter et al., 1967). Since its value is higher than the flooding limit, incomplete wetting of the fin surface is expected. The onset of liquid entrainment in upward and downward annular flow was estimated at 9.3×10^{-4} and 7.75×10^{-4} kmol/s, respectively (Hewitt and Hall-Taylor, 1970, pp. 136, 141). Since the entrainment flow rates are also larger than the flooding limit, the upper limit of operation was set at the flooding point. The upper limit for laminar flow of the vapor ($Re = 1{,}000$) was estimated at 6.2×10^{-5} kmol/s. Since its value is not far from the flooding limit, no lower limit of operation was set.

The flow sheet of the experimental unit is the same as that for our previous wetted-wall experiments (Davis et al., 1984) except that a pressure transducer was installed to measure the pressure drop along the length of the column during the operation.

Comparison of Results

In order to ensure the quality of the experimental data, each experiment was checked by computing the energy balance closure around the plate-fin device. Table 2 summarizes operating conditions and energy balance closures of the adiabatic and nonadiabatic experiments. The maximum imbalance is 11% of the total energy input to the plate-fin device and the average imbalance is 4%. A total of 17 runs were selected.

NTU profile

The desired model should consider the heat and mass transfer simultaneously along the length of the column. Therefore, the comparison between experimental and predicted results was made based upon NTU profiles and flow rate ratios. The former reflects the mass transfer behavior and the latter reflects the heat transfer behavior. An NTU profile was considered superior to a composition profile in this analysis for two reasons. First, the top and bottom compositions of *n*-hexane were generally close to 1 or 0, i.e., they are close to the pinch points in the phase-equilibrium diagram. Around these regions, it generally requires a large number of NTU's for a small change in composition. Therefore, an NTU profile serves as a more sensitive index

Table 2. Operating Conditions in Plate-Fin Experiments

Run No.	Pressure/ Pressure Drop $N/m^2, \times 10^5$	Reboiler Duty W	Wall Heat Duty W	Composition Top	Composition Bot	Reflux Rate	Reboiler Vapor Flow Rate Data	Reboiler Vapor Flow Rate Theory	Energy Flow Closure Imbalance W	Energy Flow Closure Imbalance %
				mol frac.		Rate: kmol/s, $\times 10^{-5}$				
Adiabatic										
39	1.279/0.013	1,120	0	0.980	0.480	3.352	3.097	3.242	46.8	4.52
40	1.317/0.081	1,790	0	0.966	0.396	5.136	4.924	4.765	143.0	8.51
41	1.245/0.026	1,460	0	0.964	0.430	4.086	3.987	3.834	139.0	10.26
43	1.317/0.020	1,790	0	0.886	0.010	4.836	4.872	3.768	155.0	9.58
63	1.317/0.094	1,790	0	0.743	0.051	5.023	4.853	3.996	39.9	2.46
Evaporation										
48	1.276/0.051	1,120	560	0.321	0.001	4.233	3.002	2.016	88.4	5.69
49	1.220/0.076	1,120	700	0.359	0.001	5.215	3.005	2.365	−83.7	−4.93
53	1.320/0.028	1,120	560	0.757	0.005	4.515	2.997	1.883	118.9	7.66
54	1.355/0.050	1,120	700	0.736	0.007	5.411	3.019	2.206	−27.6	−1.63
55	1.248/0.023	1,120	360	0.970	0.148	4.028	2.938	2.645	138.6	10.33
56	1.314/0.023	1,120	560	0.964	0.108	5.059	2.940	2.885	31.5	2.04
Condensation										
60	1.179/0.057	1,790	−1,100	0.987	0.117	1.897	4.794	3.695	−12.4	−0.75
62	1.155/0.075	1,790	−700	0.974	0.085	2.847	4.809	4.904	98.3	5.94
67	1.034/0.059	1,790	−1,490	0.885	0.015	0.581	4.877	4.628	−8.55	−0.52
68	1.231/0.075	1,790	−350	0.973	0.323	3.914	4.858	4.796	136.2	8.12
71	1.172/0.055	1,790	−1,100	0.982	0.068	1.599	4.448	5.220	−68.1	−4.51
72	1.089/0.060	1,790	−1,120	0.974	0.046	1.890	4.838	5.401	−45.1	−2.75

than a composition profile. Secondly, because an NTU profile is generally more linear than the composition profile along the length of the column, entrance effects are more easily detected.

Predicted curves were obtained by integrating from the column top to column bottom. A "smoothed" boundary composition was obtained by the following procedure:

1. Calculate experimental NTU profile.
2. Obtain a smoothed experimental NTU profile with a linear least-squares fit of the data.
3. Calculate vapor composition at the column top from the smoothed NTU profile.

The vapor temperature at the column top was assumed to be the dew point of the smoothed boundary vapor composition. If the difference between the dew point and bubble point temperatures exceeded 5 K, it became necessary to lower the boundary vapor temperature to obtain a reasonable vapor temperature profile. Otherwise, the calculated vapor temperature profile would rise quickly above the experimental profile as we integrated down the column. A reduction in the vapor temperature by 10% of the temperature difference between the dew point and bubble point was found to be satisfactory. The difficulty did not arise when integrating from the bottom to the top. However, because the bottom boundary conditions were subject to more severe entrance effects, integration from the bottom was not

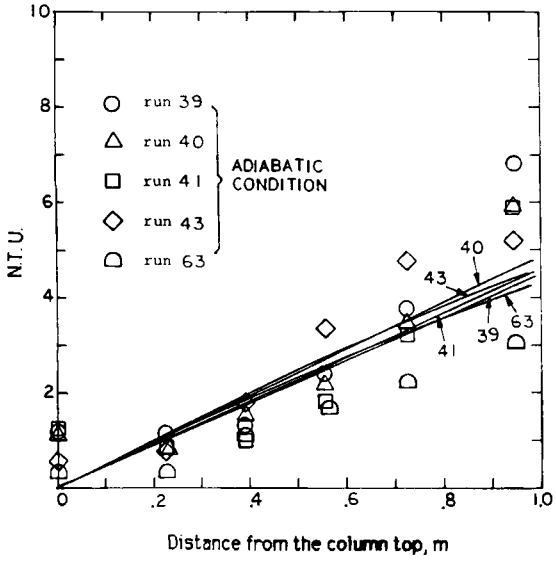

Figure 4. NTU profiles in plate-fin adiabatic fractionation.

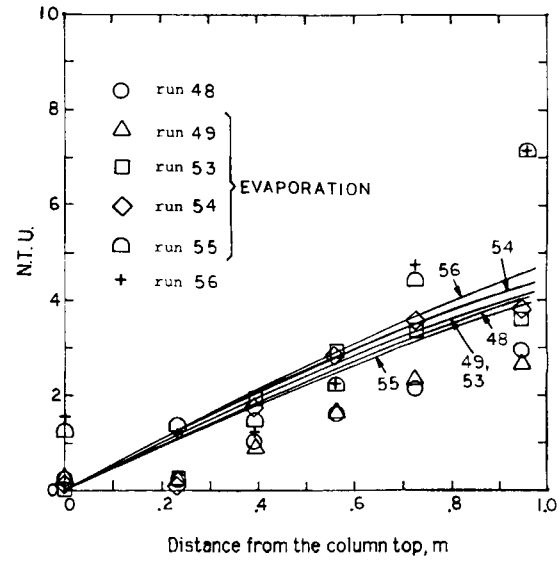

Figure 5. NTU profiles in plate-fin fractionation evaporation.

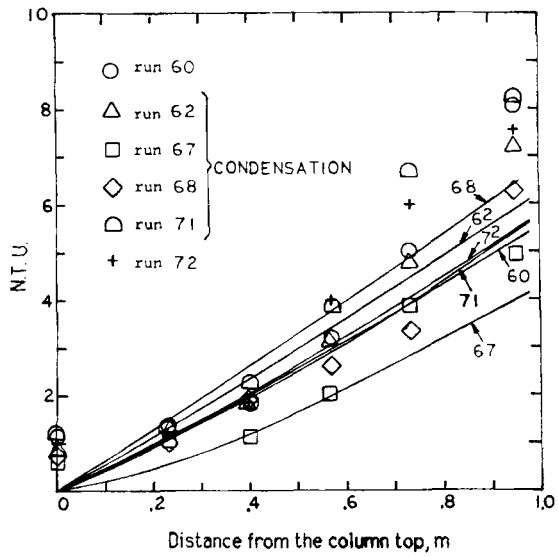

Figure 6. NTU profiles in plate-fin fractionation condensation.

desirable. It is not clear why the behavior of the calculated temperature profile would depend on the direction of integration. It is also not clear why a reduction in the boundary vapor temperature is necessary under certain conditions.

Figures 4–7 show the comparison between calculated and experimental NTU profiles. A close look at these figures reveals that the experimental NTU profile generally resembles a concave curve. The largest increase in NTU typically occurred at the bottom of the column, and the smallest increase or even a decrease of NTU occurred at the top. The bottom increase is believed to be caused by entrance effects. At this point vapor entering the column and first contacting the liquid increases the heat and mass transfer rates. On the other hand, a small increase at the top is believed to be caused by liquid maldistribution and/or entrainment, which reduce the wetted fin surface and therefore reduce the heat and mass transfer rates. Thus, it is

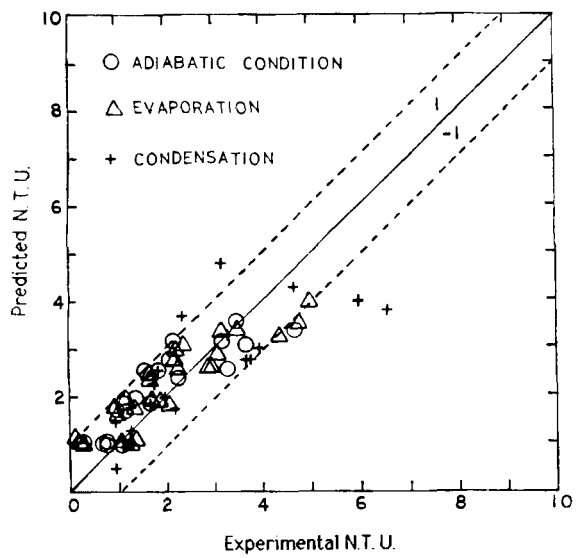

Figure 7. Comparison of experimental NTU and predicted NTU.

expected that the theory underpredicts the variation of NTU at the lower part of the column and overpredicts the variation of NTU at the upper part. The trend can be clearly observed in the figures.

Quantitatively, the smoothing procedure was used to reduce the effects on the integration of nonideal entrance conditions. If we exclude the top and bottom data points, which are subject to entrance effects, we observe that most data points are enclosed in ±1 NTU envelop along the 45 degree line (Figure 7). Individually, good agreement was found for runs 39, 40 (adiabatic), 60, and 62 (condensation), with deviation less than 0.3 NTU along the length of the column. For runs 41, 63 (adiabatic), 48, 49, 53, 54 (evaporation), and 68 (condensation), the theory generally overpredicts the NTU along the column length by about 0 to 1 NTU, indicating that a better agreement can be obtained by lowering the boundary conditions for integration. For runs 67, 71, and 72 (condensation), the theory generally underpredicts the NTU by about the same magnitude, indicating that a better agreement can be obtained by raising the boundary conditions. A plausible explanation can be given as follows: During the adiabatic and evaporation runs, and possibly condensation runs with low wall heat flux, maldistribution, and/or entrainment dominates over the bottom entrance effects because higher flow rates occur at the top of the column, hence the boundary conditions for integration are raised. During the condensation runs, the bottom entrance effects dominates over the top entrance effects because lower flow rates occur at the top of the column, hence the boundary conditions for integration are lowered. Since this does explain why we obtain good agreement for runs 39, 40, 60, and 62, other factors such as composition and temperature can also be important. At the moment we have not developed a valid formula to estimate the top and bottom entrance effects properly. For runs 43 (adiabatic), 55, and 56 (evaporation), the deviation is about ±1 NTU along the length of the column. Neither raising nor lowering the boundary conditions seems to improve the agreement.

Flow rate ratio

The flow rate ratio is defined as the ratio of reboiler vapor flow rate to reflux flow rate. Thus the flow rate ratio is representative of the heat transfer behavior of the model. A comparison of predicted and experimental results is shown in Figure 8; individual values of reboiler vapor flow rates and reflux flow rates are listed in Table 2.

From Figure 8 good agreement is observed for condensation and adiabatic runs. The deviation is about 5–10%. For the evaporation runs, approximately a 25% deviation is observed. This deviation is believed to be caused by the assumption of a negligible wall heat flux at the the dry fin surface. During the evaporation experiments, the external heat was supplied by the electric heater. Since the heater maintains the heat flux, neglecting the wall heat flux through the dry fin surface would result in a higher calculated evaporation rate of the liquid, and therefore a lower flow rate ratio. If the external heat is supplied or removed by another fluid, the deviation is expected to be much less, as in the condensation experiments.

Closing Remarks

It should be pointed out that the assumptions of constant wall heat flux and constant wall temperature have also been tried in our study. However, the agreement of both the NTU profile and

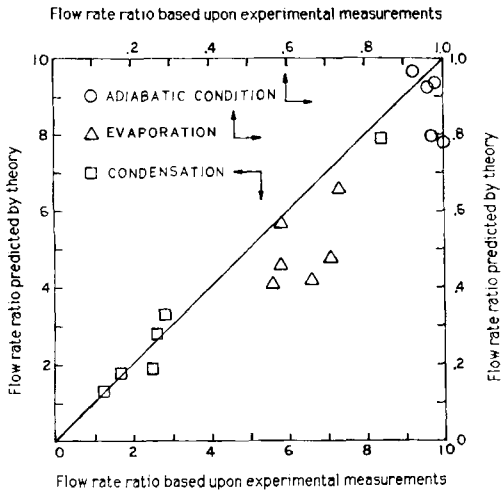

Figure 8. Comparison of flow rate ratio in plate-fin fractionation.

flow rate ratio are generally worse. Also, the constant wall heat flux assumption generally yielded extremely high dry-wall temperatures for the evaporation conditions, whereas the constant wall temperature assumption yielded dry-wall temperatures for condensation that were well below the dew point temperature. For these reasons, Eq. 22 was used.

The proposed model represents a more realistic approach than the wetted-wall model. It includes wetted ratio, wall heat flux distribution, and fin efficiency that allow us to estimate heat and mass transfer behavior in an extended surface device under adiabatic or nonadiabatic conditions easily. Due to its simplicity and generality, it may very well be extendable to other types of devices.

Acknowledgment

This work was supported by National Science Foundation Grant No. CPE 8120564.

Notation

A = column cross sectional area in the bulk flow direction, m^2
a_f = total fin surface area per unit volume of the device, $1/m$
c_p = heat capacity, J/k_gK
D = mass diffusivity, m^2/s
d = hydraulic diameter, m
e = vapor-liquid interfacial energy flux, J/m^2s
g = gravitational acceleration, m/s^2
H = vapor molar enthalpy, $J/kmol$
HTU = height of transfer unit, column length/NTU's
h = liquid molar enthalpy, $J/kmol$
h = heat transfer coefficient, W/m^2K
k = mass transfer coefficient, $kmol/m^2s$
L = downward liquid molar flow rate, $kmol/s$
l = fin strip length, m
M = molecular weight, $kg/kmol$
NTU = number of transfer unit, $\int dy/(y_i - y)$
n = interfacial molar flux, $kmol/m^2s$
p = pressure, Pa
Pr = Prandtl number, $\mu c_p/\kappa$
q_w = wall heat flux, W/m^2
Re = Reynolds number, WdM/μ
Sc = Schmidt number, $\rho D/\mu$
T = vapor temperature, K
t = liquid temperature, K
V = upward vapor molar flow rate, $kmol/s$
W = vapor molar flux in the z direction, $kmol/m^2s$
x = mole fraction of the more volatile component in the liquid phase
y = mole fraction of the more volatile component in the vapor phase
z = coordinate in the bulk flow direction

Greek letters

Γ = minimum wetting rate, $kmol/ms$
γ = surface tension, kg/s^2
η = fin efficiency, Eq. 8
θ = contact angle, degree or radian
κ = thermal conductivity, $W/m \cdot K$
λ = latent heat, $J/kmol$
μ = viscosity, kg/ms
ν = kinematic viscosity, m^2/s
ρ = density, kg/m^3
ω = wetted ratio, defined as the ratio of wetted fin surface area over total fin surface area

Subscripts

dry = dry region
f = fin
g = gas
i = interface
l = liquid
w = wall
wet = wet region
1 = component 1, more volatile component
2 = component 2, less volatile component

Superscript

* = corrected transfer coefficient

Literature Cited

Bankoff, S. G., and H. H. Tung, "Rivulets Formation on a Heated Wall," *Heat Transfer, Proc. 7th Int. Heat Conf.*, 363 (1982).

Burmester, L. C., "Vertical Fin Efficiency with Film Condensation," *Trans. ASME, J. Heat Transfer*, **104**, 391 (1982).

Chapman, A. J., "Working Formulae and Dimensionless Correlations for Forced Convection," *Heat Transfer*, Macmillan, New York, Ch. 8 (1974).

Davis, J. F., H. H. Tung, and R. S. H. Mah, "Fractionation with Condensation and Evaporation in Wetted-Wall Columns," *AIChE J.* **30**, 328 (1984).

Fitzmorris, R. E., and R. S. H. Mah, "Improving Distillation Column Design Using Thermodynamic Availability," *AIChE J.* **26**, 265 (1980).

Fujuta, T., and T. Ueda, "Heat Transfer to Falling Films and Film Breakdown," *Int. J. Heat Mass Transfer*, **21**, 97 (1978).

Haselden, G. G., W. A. Platt, and A. Wahhab, "The Development of an Efficient Fractionating Condenser," *Trans. Inst. Chem. Eng.*, **38**, 46 (1960).

Henley, E. J., and J. D. Seader, *Equilibrium-Stage Separation Operation in Chemical Engineering*, Wiley, New York (1981).

Hewitt, G. F., and N. S. Hall-Taylor, *Annular Two-Phase Flow*, Pergamon (1970).

Kern, D. Q., and A. D. Kraus, *Extended Surface Heat Transfer*, McGraw-Hill, New York (1972).

Mah, R. S. H., "Performance Evaluation of Distillation Systems," *Foundations of Computer-Aided Chemical Process Design*, R. S. H. Mah and W. D. Seider, eds., Engineering Foundation and AIChE (1981).

Mah, R. S. H., J. J. Nicholas, Jr., and R. B. Wodnik, "Distillation with Secondary Reflux and Vaporization: A Comparative Evaluation," *AIChE J.* **23**, 651 (1977).

Mikielewicz, J., and J. R. Moszynski, "Minimum Thickness of a Liquid Film Flowing Vertically Down a Solid Surface," *Int. J. Heat Mass Transfer*, **19**, 771 (1976).

Nader, W. K., "Extended Surface Heat Transfer with Condensation," Paper CS-5, *6th Int. Heat Transfer Conf.*, Toronto (Aug., 1978).

Patankar, S. V., and E. M. Sparrow, "Condensation on an Extended Surface," *Trans. ASME, J. Heat Transfer*, 434 (Aug., 1979).

Platt, W. A., and G. G. Haselden, "Individual and Overall Mass Transfer Coefficients for Overflow Packing," *Trans. Inst. Chem. Eng.*, **43**, 92 (1965).

Ponter, A. B., et al., "The Influence of Mass Transfer of Liquid Film Breakdown," *Int. J. Heat Mass Transfer*, **10**, 349 (1967).

Puranik, S. S., and A. Vogelpohl, "Effective Interfacial Area in Irrigated Packed Column," *Chem. Eng. Sci.*, **29**, 501 (1974).

Rao, D. S., and M. S. Murthy, "Heat Transfer during Dropwise Condensation," *Chem. Eng. J.*, **26**, 1 (1983).

Schluter, L., and R. Schmidt, "A Present Trend in Rectification, Energy Saving," *Int. Chem. Eng.*, **23**, 427 (1983).

Sparrow, E. M., R. B. Baliga, and S. V. Patankar, "Analysis of Interrupted-Wall Channels, with Application of Heat Exchangers," *Trans. ASME, J. Heat Transfer*, 4 (Feb., 1977).

Tung, H. H., "Fractionating Condensation and Evaporation in Continuous-Contact Devices and Application to SRV Distillation," Ph.D Diss., Northwestern Univ. (1985).

Watanabe, K., and T. Munakata, "Distillation Performance of Externally Heated or Cooled Differential Contacting Column," *J. Chem. Eng. Japan*, **9**, 113 (1976).

Weiting, A. R., "Empirical Correlations for Heat Transfer and Flow Friction Characteristics of Rectangular Offset-Fin Plate-Fin Heat Exchangers," *Trans. ASME, J. Heat Transfer*, 488 (Aug., 1975).

Winteringham, R., and G. G. Haselden, "An Approach to Thermodynamic Reversibility in the Fractionation of Liquid Air," *Trans Inst. Chem. Eng.*, **44**, 55 (1966).

Manuscript received July 9, 1985, and revision received Nov. 6, 1985.